

## ON THE ORIGIN OF THE $\gamma$ -RAY/OPTICAL LAGS IN LUMINOUS BLAZARS

MATEUSZ JANI<sup>1</sup>, MAREK SIKORA<sup>1</sup>, KRZYSZTOF NALEWAJKO<sup>2</sup>, RAFAŁ MODERSKI<sup>1</sup>, AND GREG M. MADEJSKI<sup>3</sup>

*accepted for publication in The Astrophysical Journal*

### ABSTRACT

Blazars are strongly variable sources that occasionally show spectacular flares visible in various energy bands. These flares are often, but not always, correlated. In a number of cases the peaks of optical flares are found to be somewhat delayed with respect to the gamma-ray peaks. One notable example of such a delay was found in 3C 279 by Hayashida et al. and interpreted as a result of steeper drop with distance of the energy density of external radiation field than of the magnetic energy density. In this paper we demonstrate that in general, depending on the respective energy density profile along the jet, such lags can have both signs and that they can take place for any ratio of these energy densities. We study the dependence of such lags on the ratio of these energy densities at a distance of a maximal energy dissipation in a jet, on their gradients, as well as on the time profile of the relativistic electron injection within the moving source. We show how prominent such lags can be, and what are their expected time scales. We suggest that studies of such lags can provide a powerful tool to resolve the structure of relativistic jets and their radiative environment. As an example we model the lag observed in 3C 279, showing that in this object the flare is produced at a distance of a few parsecs from the central black hole, consistent with our previous inferences based on the spectra and optical polarization properties.

*Subject headings:* quasars: jets — radiation mechanisms: non-thermal — acceleration of particles

### 1. INTRODUCTION

Blazars are variable in all spectral bands and over a very broad range of time scales, from years down to days or sometimes even minutes (e.g., Ulrich et al. 1997; Abdo et al. 2010a; Ghisellini & Tavecchio 2008). Largest amplitude variations are detected in the gamma-ray band (Abdo et al. 2010a). In luminous blazars, belonging to the class of Flat-Spectrum Radio Quasars (FSRQs), the gamma-ray light curves usually correlate with the optical light curves (Chatterjee et al. 2012), but with the peaks of short-term flares sometimes delayed with respect to each other (Wagner et al. 2009). In particular, gamma-ray flares leading the optical flares by a few days have been indicated in several blazars — PKS 1510-089 (Abdo et al. 2010b; D’Ammando et al. 2011), PKS 1502+106 (Abdo et al. 2010c), AO 0235+164 (Agudo et al. 2011; Ackermann et al. 2012), and 3C 279 (Hayashida et al. 2012).

Such lags are very intriguing because, according to the most commonly accepted external-radiation-Compton (ERC) models, radiation in the optical and  $\gamma$ -ray bands is produced by electrons with similar energies and deeply in the fast cooling regime (i.e. electron cooling time scale is much shorter than the source light-crossing time scale). In such case, lags cannot result from the difference in cooling time scales, as in the scenarios considered by Sikora et al. (2001) and Sokolov & Marscher (2005). Hayashida et al. (2012) suggested that the optical/ $\gamma$ -ray lags may result from different distance dependencies

of the magnetic energy density and the energy density of external diffuse radiation field. Here we explore this possibility in detail, studying the dependence of the lag properties on such model parameters as gradients of the energy densities, the electron injection time profile, and the ERC-to-synchrotron flux ratio at the distance of the maximum electron injection rate.

Our paper is structured as follows. In Section 2, we describe our model of synchrotron/ERC flares that allows us to study the  $\gamma$ -ray/optical lags, and study how the resulting lag parameters depend on the details of the model. In Section 3, we apply our model to luminous blazars with dense radiative environment, and to the particular case of 3C 279. A further discussion and conclusions are given in Section 4.

### 2. MODELING THE LAGS

#### 2.1. Assumptions and equations

Assuming that the source of a non-thermal flare propagates down the jet with a constant velocity, we can describe its activity as a function of its distance from the black hole,  $r = ct'\Gamma$ , where  $t'$  is the time measured in the source co-moving frame and  $\Gamma$  is the bulk Lorentz factor of the jet. We investigate light curves produced by electrons deeply in the fast cooling regime by the synchrotron and ERC processes. They are determined assuming that the observed time scale of light-travel effects caused by the finite size of a source is much shorter than the observed time scale of the source propagation. Such assumption is justified by observations suggesting that the AGN jet semi-opening angles are smaller than the Doppler angles (e.g. Pushkarev et al. (2009)). The ERC process is treated in the Thomson regime, using the following approximate formula (Moderski et al. 2003):

$$[\nu F_{\text{ERC},\nu}]_{\nu=\nu_{\text{HE}}}(t_{\text{obs}}) \propto [\gamma N_{\gamma}|\dot{\gamma}|_{\text{ERC}}](r), \quad (1)$$

<sup>1</sup> Nicolaus Copernicus Astronomical Center, Bartyccka 18, 00-716 Warsaw, Poland; [mjaniak@camk.edu.pl](mailto:mjaniak@camk.edu.pl), [msikora@camk.edu.pl](mailto:msikora@camk.edu.pl)

<sup>2</sup> University of Colorado, UCB 440, Boulder, CO 80309, USA

<sup>3</sup> Kavli Institute for Particle Astrophysics and Cosmology, SLAC National Accelerator Laboratory, Stanford University, 2575 Sand Hill Road M/S 29, Menlo Park, CA 94025, USA

for the electron Lorentz factor satisfying  $\gamma^2 \simeq (1 + z)\nu_{\text{HE}}/(\mathcal{D}^2\nu_{\text{ext}})$ , where  $\nu_{\text{HE}}$  is the observed frequency of the high-energy component,  $\nu_{\text{ext}}$  is the average frequency of the external diffuse radiation field,  $N_\gamma$  is the electron energy spectrum,  $|\dot{\gamma}|_{\text{ERC}} \propto \gamma^2 u'_{\text{ext}}(r)$  is the rate of the electron energy losses via the ERC process,  $u'_{\text{ext}}(r)$  is the energy density of external radiation field as measured in the source comoving frame,  $t_{\text{obs}} = r/(\mathcal{D}\Gamma c)$  is the observation time,  $\mathcal{D} = 1/[\Gamma(1 - v \cos \theta_{\text{obs}}/c)]$  is the Doppler factor, and  $z$  is the source redshift.

The synchrotron flux is approximated in an analogous way by

$$[\nu F_{\text{syn},\nu}]_{\nu=\nu_{\text{LE}}}(t_{\text{obs}}) \propto [\gamma N_\gamma |\dot{\gamma}|_{\text{syn}}](r), \quad (2)$$

for the electron Lorentz factors  $\gamma^2 \simeq 3\pi(1 + z)m_e c \nu_{\text{syn}}/[2eB'(r)]$ , where  $\nu_{\text{LE}}$  is the observed frequency of the low-energy spectral component,  $|\dot{\gamma}|_{\text{syn}} \propto \gamma^2 u'_B(r)$  is the rate of the electron energy losses via the synchrotron process, and  $u'_B(r) = B'(r)^2/(8\pi)$  is the energy density of the magnetic field carried by the source. Assuming a power-law injection function  $Q_\gamma = K(r)\gamma^{-p}$ , where  $K(r)$  has a maximum at  $r = r_m$ , one can find that deeply in the electron fast cooling regime

$$N_\gamma = \frac{\int_\gamma Q_\gamma d\gamma}{|\dot{\gamma}|_{\text{rad}}} \propto \frac{\int_\gamma Q_\gamma d\gamma}{\gamma^2(u'_B + u'_{\text{ext}})} \propto \frac{K(r)\gamma^{-p-1}}{(u'_B + u'_{\text{ext}})}, \quad (3)$$

where we ignore radiative losses due to the synchrotron self-Compton (SSC) process.

Combination of (3), (1), and (2) gives

$$[\nu F_{\text{ERC},\nu}]_{\nu=\nu_{\text{HE}}} \propto \gamma^{-p+2} K(r) \frac{u'_{\text{ext}}(r)}{u'_{\text{ext}}(r) + u'_B(r)}, \quad (4)$$

$$[\nu F_{\text{syn},\nu}]_{\nu=\nu_{\text{LE}}} \propto \gamma^{-p+2} K(r) \frac{u'_B(r)}{u'_{\text{ext}}(r) + u'_B(r)}. \quad (5)$$

For particular spatial distributions of the energy densities  $u'_{\text{ext}}(r) \propto r^{-\beta_E}$  and  $u'_B(r) \propto r^{-\beta_B}$ , we obtain that the ERC and synchrotron light curves are

$$F_{\text{ERC},\nu_{\text{HE}}}(x) \propto K(x) \frac{q_m}{q_m + x^{\Delta\beta}}, \quad (6)$$

and

$$F_{\text{syn},\nu_{\text{LE}}}(x) \propto x^{-(p-2)\beta_B/4} K(x) \frac{x^{\Delta\beta}}{q_m + x^{\Delta\beta}}, \quad (7)$$

where  $q_m = u'_{\text{ext}}(r_m)/u'_B(r_m)$ ,  $x = r/r_m$ , and  $\Delta\beta = \beta_E - \beta_B$ .<sup>4</sup>

In order to compute the light curves, we need to specify the electron injection function  $K(x)$ . We choose a modified Gaussian function

$$K(x) = x \cdot \exp\left[-\frac{(x-1)(x+\sigma^2-1)}{\sigma^2}\right] \quad (8)$$

with a ‘dispersion’  $\sigma$  and the property that  $K(x) \rightarrow 0$  for  $x \rightarrow 0$ .

<sup>4</sup> Note that the factor  $x^{-(p-2)\beta_B/4}$  in the latter equation results from the fact that in the synchrotron process  $\gamma \propto 1/\sqrt{B(r)'} \propto r^{\beta_B/4}$ .

## 2.2. Light curves

Equations (6), (7) and (8) show that the number of free parameters determining the light curves is: 3 for the ERC case ( $q_m$ ,  $\Delta\beta$  and  $\sigma$ ); and 5 for the synchrotron case (the two additional parameters are  $\beta_B$  and  $p$ ). The number of free parameters determining the synchrotron light curve can be reduced to 3 by assuming the electron injection function index of  $p = 2$ . Noting that electrons injected with such an index in the fast cooling regime produce spectra with the index  $\alpha = p/2 = 1$  ( $F_\nu \propto \nu^{-\alpha}$ ), and that  $\alpha \sim 1 - 1.4$  are typical slopes of synchrotron spectra of luminous blazars (Ledden & Odell 1985), we consider this choice to be representative, and, with the exception of Section 2.4, we limit our further investigations to the case of  $p = 2$ .

Before plotting some examples of the light curves and their dependence on the model parameters, we can deduce the main features of the light curves directly from Eqs (6) and (7). We can see that:

1. For  $\Delta\beta = 0$ , the ERC and synchrotron light curves follow the shape of the electron injection function and both peak at  $x = 1$  (zero lag);
2. From the ratio of the two light curves ( $\propto x^{\Delta\beta}$ ) one can deduce that for  $\Delta\beta > 0$  the ERC peak precedes the synchrotron one (hereafter we call it the positive lag), and for  $\Delta\beta < 0$  the ERC peak is delayed relative the synchrotron one (negative lag);
3. For  $q_m \gg 1$ , the shape of the ERC flare follows the shape of the electron injection function, and therefore has a peak at  $x \simeq 1$  (it was the case studied in the Appendix to Hayashida et al. 2012). For  $q_m \ll 1$ , the synchrotron flare follows the shape of the electron injection function and has a peak at  $x \simeq 1$ .

In Figure 1, we present three plots showing the dependence of the light curves on  $q_m$ ,  $\Delta\beta$  and  $\sigma$ . We can see that  $q_m$  determines mainly the location of the flare peaks relative to the point  $x = 1$ , while  $\sigma$  and  $\Delta\beta$  determine mainly the distance between peaks and the flare symmetry.

## 2.3. The length and prominence of a lag

We define the lag length as

$$\Delta x_{\text{lag}} = x_{\text{syn}} - x_{\text{ERC}}, \quad (9)$$

(see Fig. 2) where  $x_{\text{ERC}}$  and  $x_{\text{syn}}$  are the locations where the ERC and synchrotron peaks are produced. The dependence of  $\Delta x_{\text{lag}}$  on  $q_m$ ,  $\Delta\beta$  and  $\sigma$  is presented in Fig. 3. One can see that for  $\sigma = 0.6$ ,  $\Delta\beta = 4$  and  $q_m > 1$ , the lag length reaches the value of  $\Delta x_{\text{lag}} \sim 0.4$  and may be much higher for higher values of  $\sigma$ .

However, as one can see from Fig. 1, even for very large lag lengths the flares overlap significantly and are not strongly contrasted. To verify for which model parameters are these lags reasonably prominent, we introduce two parameters to quantify the lag ‘prominence’ (see Fig. 2):<sup>5</sup>

$$C_{\text{ERC}} = \frac{F_{\nu,\text{HE}}(x_{\text{ERC}}) - F_{\nu,\text{HE}}(x_{\text{syn}})}{F_{\nu,\text{HE}}(x_{\text{ERC}})} \quad (10)$$

<sup>5</sup> Note that our choice of description of the lag prominence with two parameters is dictated by practical reasons. Because of typ-

and

$$C_{\text{syn}} = \frac{F_{\nu, \text{LE}}(x_{\text{syn}}) - F_{\nu, \text{LE}}(x_{\text{ERC}})}{F_{\nu, \text{LE}}(\gamma)(x_{\text{syn}})}. \quad (11)$$

The dependence of these indicators on the model parameters is presented in Fig. 4. We find that both measures of the lag prominence increase with increasing  $\Delta\beta$  and increasing  $\sigma$ . The dependence on  $q_m$  is more complex – for  $q_m \lesssim 1$  the lag prominence decreases with increasing  $q_m$ , while for  $q_m \gg 1$  the lag prominence depends on  $q_m$  very weakly.

#### 2.4. The case of $p \neq 2$

In Figure 5, we show the dependence of the lag length on the injected electron energy distribution index  $p$ . We can see that regardless of the value of  $\Delta\beta$ , the lag length slightly decreases with increasing  $p$ . This means that the absolute value of the lag decreases for positive lags and increases for negative lags. This can be easily understood from the existence of a factor  $x^{-(p-2)\beta_B/4}$  in Eq. (7).

### 3. APPLICATIONS

We have studied basic features of lags between the ERC and synchrotron light curves produced in the fast cooling regime. Our model shows that the presence of such lags is made possible by a non-zero value of  $\Delta\beta$  which corresponds to a significant change of the Compton dominance parameter  $q = u'_{\text{ext}}/u'_B \propto r^{-\Delta\beta}$  within the distance range of enhanced activity of the propagating source. In a quasar radiative environment the change of  $q$  with distance is expected to result mainly from the strong stratification of the external radiation field sources, being connected with broad-line region (BLR) and hot-dust region (HDR). Changes of  $q$  with distance can be deduced from Fig. 6, where radial distributions of respective energy densities are schematically presented (see also Sikora et al. 2009). In this figure we marked regions where  $q$  decreases with a distance (region “I”) and regions where  $q$  increases with a distance (region “II”). Hence, positive lags ( $t_\gamma < t_{\text{opt}}$ ) are expected to be produced in regions “I,” and negative lags are expected to be produced in regions “II.”

Since optimal conditions for production of prominent lags are such that the distance range of enhanced source activity determined by  $x \sim \sigma$  coincides with the region of largest changes of  $q$ , one may expect that observed lags,  $\Delta t_{\text{lag}}$ , are produced at distances  $r_m \sim \Delta r_{\text{lag}} \simeq c\Delta t_{\text{lag}} \mathcal{D}\Gamma/(1+z)$ . Hence, when observing a lag of  $\Delta t_{\text{lag}}$ , one can estimate  $r_m$  and locate the source activity relative to  $r_{\text{BLR}}$  and  $r_{\text{HDR}}$ , which values can be estimated from the broad line luminosities and the hot dust sublimation temperatures (see Sikora et al. 2009 and refs. therein). Unfortunately, due to limited effective area of present  $\gamma$ -ray instruments (such as *Fermi*-LAT) it is possible to construct light curves with data quality only sufficient to verify the presence of correlation between optical and  $\gamma$ -ray data and estimate lag length only with time resolution longer than a day (with exception of the very brightest  $\gamma$ -ray sources). Noting that in luminous

blazars  $r_{\text{BLR}} \sim 10^{18}$  cm, and that the observed time of the propagation of the source over the distance range of this order is  $\sim 1.7(1+z)/(\Gamma/20)^2$  days, presently only lags produced in the HDR have a chance to be probed observationally.

To verify the applicability of our lag model, we use it to match the data on blazar 3C 279 presented by Hayashida et al. (2012) (see also Abdo et al. 2010d). A light curve analysis presented in their paper (R-band vs.  $\gamma$ -rays of energies  $> 200$  MeV) with the discrete-correlation-function method showed a peak at +10 days, indicating a presence of a positive lag of that length. We used their data from the time interval MJD 54870-900 including representative strong flares in optical/ $\gamma$ -ray bands, and made an attempt to model them with the flare profiles given in Sec. 2.1. The data and the model light curves are presented in Fig. 7. The parameters of our model are:  $q_m = 30$ ,  $\beta_B = 2$ ,  $\beta_E = 5$ ,  $\sigma = 1$ ,  $r_m = 4.4$  pc and  $\Gamma = 10$ . These results are consistent with the ERC model parameters used by Hayashida et al. (2012) to fit the broad band spectra of 3C 279. We would like to emphasize that the presence of a +10 days lag in the case of 3C 279 is just a possibility as the used analysis might have been misled by poor data quality. Our choice of the strong flares from the whole lightcurve presented in Hayashida et al. (2012) is therefore just an example indicating that the model can be applied to a real data with very reasonable parameters.

### 4. DISCUSSION AND CONCLUSIONS

In rarefied magnetized plasmas of astrophysical non-thermal sources, dissipative processes often generate short-term bursts of relativistic electrons, which in turn produce synchrotron and inverse-Compton flares. Provided that the energy density of seed photons, measured in the source co-moving frame, is dominated by external sources, the inverse-Compton radiation is dominated by the ERC process. For quasi-uniform energy densities of magnetic and seed radiation fields across the source, and for electrons energies such that the time scale of their radiative cooling is much shorter than the time scale of the burst, the synchrotron and ERC flare profiles will follow the electron injection function shape almost exactly, without any lags. At the same time, the flux ratio of the two spectral components will approximately be scaled by the ratio of energy densities of seed radiation field to magnetic field, as long as the inverse Compton scattering proceeds in the Thomson regime.

However, in blazars, the outbursts are produced by sources (e.g., internal shocks, magnetic reconnection domains) which propagate down the jet with relativistic speeds. As we illustrated in Fig. 6, in FSRQs, the energy density distribution of external radiation field is significantly stratified, while the magnetic field intensity is expected to monotonically drop with a distance due to the jet divergence. As our equations in Section 2 show, in such an environment, for sources propagating down the jet, optical light curves produced by the synchrotron mechanism differ from  $\gamma$ -ray light curves produced by the ERC process. In particular, if the source is bursting within the regions marked on Fig. 6 by “I” or “II,” we will observe flares which are delayed with respect to each other, with the  $\gamma$ -ray flares preceding the optical ones if the burst takes place at  $r_{\text{BLR}} < \Delta r_{\text{burst}} \ll r_{\text{HDR}}$

ically poor time sampling and large errors in high energy light curves, such definition enables us to estimate the lag contrast in a more precise way than using a single parameter, e.g. the flux at the intersection of two normalized flares.

and  $\Delta r_{\text{burst}} \gg r_{\text{HDR}}$ , and with the optical flares preceding the  $\gamma$ -ray ones for  $\Delta r_{\text{burst}} < r_{\text{BLR}}$  and  $r_{\text{BLR}} \ll \Delta r_{\text{burst}} < r_{\text{HDR}}$ .

Our scheme does not include the presence of a warm dust, which together with the hot phase, produces spectra extending up to  $20\,\mu\text{m} - 30\,\mu\text{m}$  (see, e.g., Fig. 7 in Shang *et al.* 2011). The observed spectra indicate a distribution of dust extending to much larger distances than  $r_{\text{HDR}}$ . In this case, the decrease of the external radiation energy density does not necessarily have to be faster than the decrease of the magnetic energy density. However, frequently observed excesses of the NIR radiation over the MIR component extrapolated to shorter wavelengths (Mor *et al.* 2009; Leipski *et al.* 2010) suggest that there can be two separate thermal components from dust, the hot one produced by graphite and located in the outer portions of the BLR, and the cooler one produced by both graphite and silicate grains and enclosed within clumps of the molecular tori extending up to tens of parsecs (Mor & Netzer 2012; Kishimoto *et al.* 2012; Roseboom *et al.* 2012). Hence, a confirmation of predominantly positive optical/ $\gamma$ -ray lags of a few days can independently support such a stratification of the dust distribution.

Obviously, the model proposed and studied by us, aimed to explain the observed lags between optical and  $\gamma$ -ray flare peaks is not a unique one, but is the only one which involves *single dissipative events*. This model can be verified in future against two-dissipative-zone scenarios, e.g. those involving reconfinement plus reflection shock structures, or two internal shocks formed independently at different locations (Katarzynski & Ghisellini 2007), by future more detailed and better resolved light curves.

We studied the dependence of synchrotron-ERC lags on model parameters which determine the distribution of magnetic and external radiation fields, their energy density ratio at the time of the electron injection peak, the dispersion of the injection function, and the slope of the injected electron spectrum. Our main results can be summarized as follows:

- Variations of  $q = u'_{\text{ext}}/u'_B$  with a distance result in different ERC and synchrotron light curves;
- Electron injection bursts produced within the region of the monotonic changes of  $q$  lead to the production of the lagged flares, positive ( $\gamma$ -ray first) for  $dq/dr < 0$ , negative for  $dq/dr > 0$ ;
- The ‘prominence’ of such lags increases with increasing burst dispersion  $\sigma$  and increasing gradients of  $q$ . The most prominent lags are expected when the burst length coincides with the region of largest gradient of  $q$ ;
- Limited time resolution of  $\gamma$ -ray data currently allows only searches for lags larger than a few days, which corresponds to distances of the order of, or larger than, the sublimation radius of the hot dust. As an example, we showed that our model light curves can be matched to the observed  $\gamma$ -ray/optical flare of 3C 279 in February 2009, when a 10-day lag was seen (Hayashida *et al.* 2012).

- Future more detailed and better resolved light curves should allow to discriminate whether the optical -  $\gamma$ -ray lags can be explained by single dissipative events, or whether two spatially separated dissipation zones must be involved.

We would like to thank the referee Fabrizio Tavecchio for critical comments which helped to improve the paper. We acknowledge financial support by the Polish NCN grant DEC-2011/01/B/ST9/04845, the NSF grant AST-0907872, the NASA ATP grant NNX09AG02G, and NASA Fermi GI grant No. NNX11AO39G. GM acknowledges DoE support to SLAC via contract No. DE-AE3-76SF00515.

## REFERENCES

- Abdo, A. A., et al. (Fermi-LAT Collaboration) 2010a, *ApJ*, 722, 520
- Abdo, A.A., et al. (Fermi-LAT Collaboration) 2010b, *ApJ*, 721, 1425
- Abdo, A.A., et al. (Fermi-LAT Collaboration) 2010c, *ApJ*, 710, 810
- Abdo, A. A., et al. (Fermi-LAT Collaboration) 2010d, *Nature*, 463, 919
- Ackermann, M., et al. (Fermi-LAT Collaboration) 2012, *ApJ*, 751, 159
- Agudo, I., Marscher, A.P., Jorstad, S.G., et al. 2011, *ApJL*, 735, L10
- Chatterjee, R., Bailyn, C. D., Bonning, E. W., et al. 2012, *ApJ*, 749, 191
- D'Ammando, F. et al. (AGILE Collaboration) 2011, *A&A*, 529, A145
- Ghisellini, G., Tavecchio, F. 2008, *MNRAS*, 386, L28
- Hayashida, M., et al. (Fermi-LAT Collaboration) 2012, *ApJ*, 754, 114
- Katarzyński, K. & Ghisellini, G. 2007, *A&A*, 463, 529
- Kishimoto, M., Hönig, S.F., Antonucci, R., et al. 2012, *Journal of Physics, Conference Series*, 372, 012033
- Ledden, J.E. & Odell, S.L. 1985, *ApJ*, 298, 630
- Leipski, C., et al. 2010, *ApJ*, 717, 766
- Moderski, R., Sikora, M., & Błażejowski, M., 2003, *A&A*, 406, 855
- Mor, R., & Netzer, H. 2012, *MNRAS*, 420, 526
- Mor, R., Netzer, H., & Elitzur, M. 2009, *ApJ*, 705, 298
- Pushkarev, A. B., et al. 2009, *A&A*, 507, L33
- Roseboom, I. G., Lawrence, A., Elvis, M., et al. 2012, arXiv:1205.4543
- Shang, Z., et al. 2011, *ApJS*, 196, 2
- Sikora, M., Błażejowski, M., Begelman, M. C., & Moderski, R. 2001, *ApJ*, 554, 1
- Sikora, M., Stawarz, L., Moderski, R., Nalewajko, K., & Madejski, G. M., 2009, *ApJ*, 704, 38
- Sokolov, A. & Marscher, A.,P. 2005, *ApJ*, 629, 52
- Ulrich, M.-H., Maraschi, L., & Urry, C.M. 1997, *ARAA*, 35, 445
- Wagner, S. J., Hauser, M., Behera, B., & Kurtanidze, O. 2009, *Fermi Symposium*

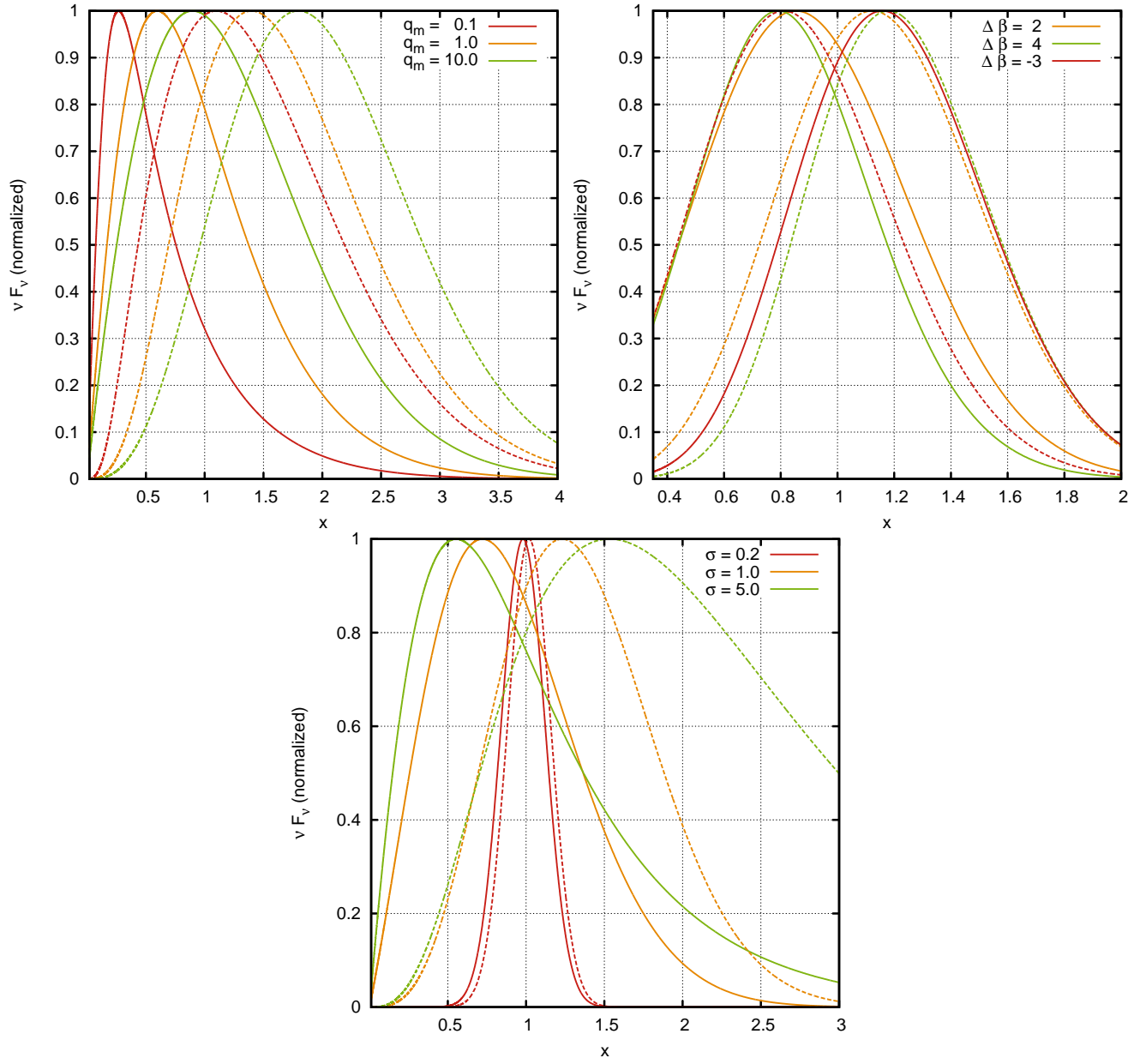


**Figure 1.** Normalized shapes of ERC flares (*solid lines*) and synchrotron flares (*dotted lines*). *Top left panel:*  $\sigma = 0.6$  and  $\Delta\beta = 2$ . *Top right panel:*  $\sigma = 0.6$  and  $q_m = 1$ . *Bottom panel:*  $\Delta\beta = 2$  and  $q_m = 1$ .

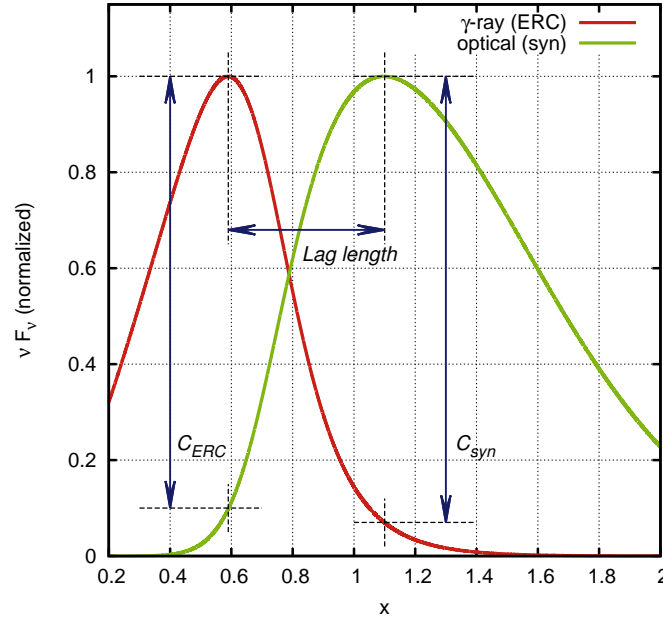


**Figure 2.** Definitions of the lag length and the two measures of lag prominence for a sample pair of normalized light curves.

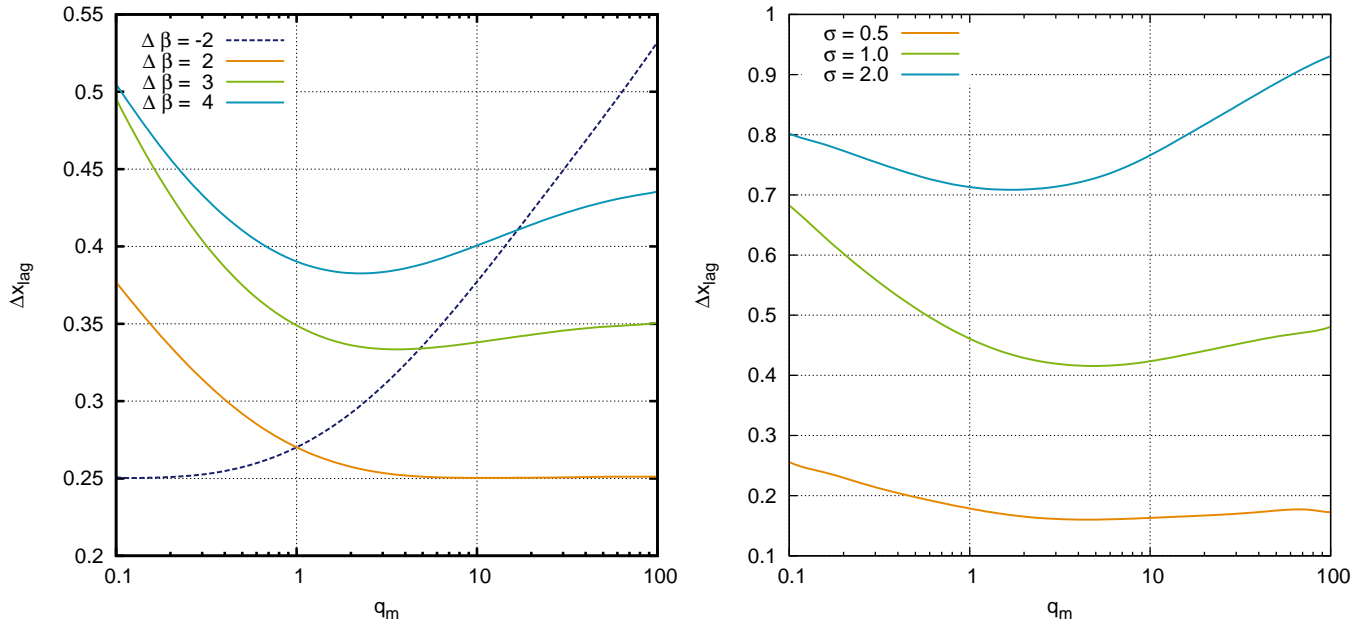


**Figure 3.** Lag length dependence on  $q_m$ . *Left panel:*  $\sigma = 0.6$ . Dotted curve, corresponding to  $\Delta\beta < 0$  (negative lag), has been flipped over x-axis. *Right panel:*  $\Delta\beta = 2$ .

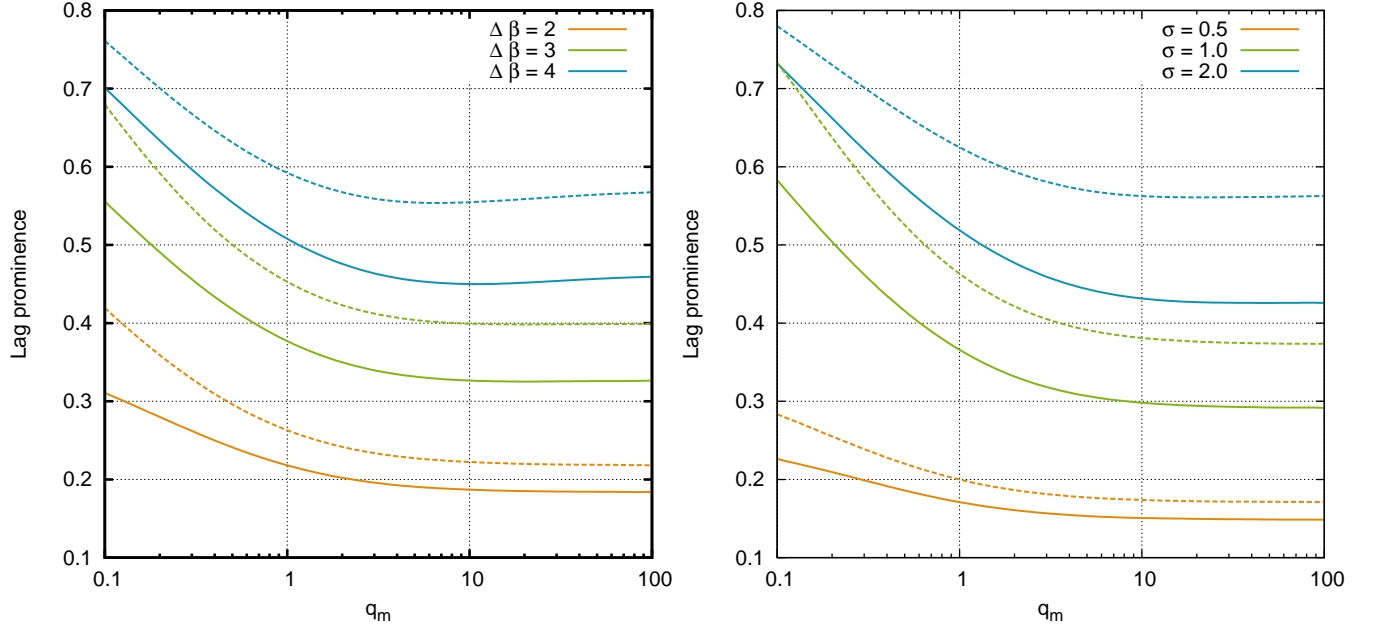


**Figure 4.** Lag prominence indicators,  $C_{\text{ERC}}$  (solid lines) and  $C_{\text{syn}}$  (dotted lines), dependence on  $q_m$ . Left panel:  $\sigma = 0.6$ . Right panel:  $\Delta\beta = 2$ .

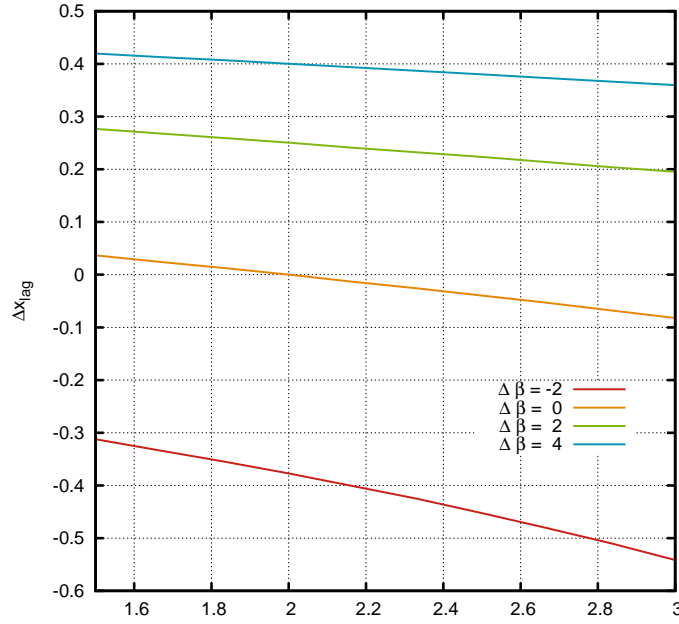


**Figure 5.** Lag length dependence on the index of the electron injection function  $p$  for  $q_m = 10$ ,  $\beta_B = 2$ ,  $\sigma = 0.6$ .



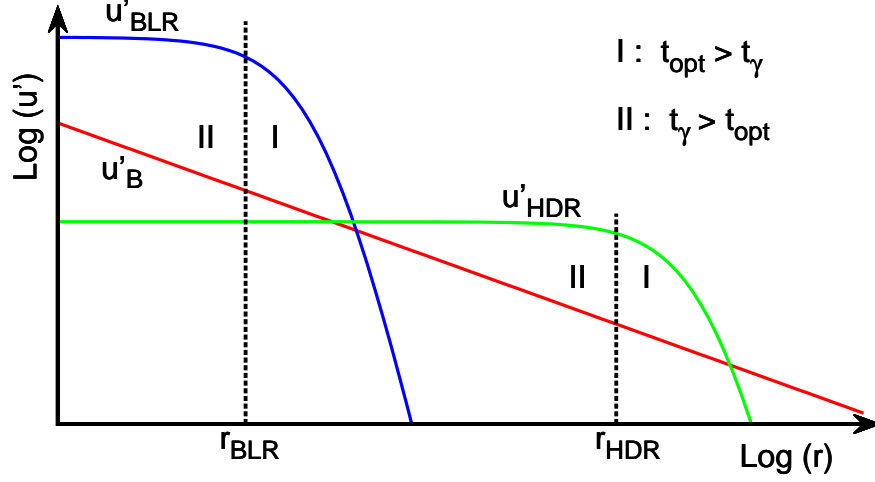


**Figure 6.** Schematic view of distance dependence of magnetic and external radiation field energy densities as measured in the source co-moving frame (see Fig. 3 in Sikora et al. 2009). Label ‘I’ marks the regions where positive lags are expected, whereas label ‘II’ corresponds to regions where negative lags are expected.

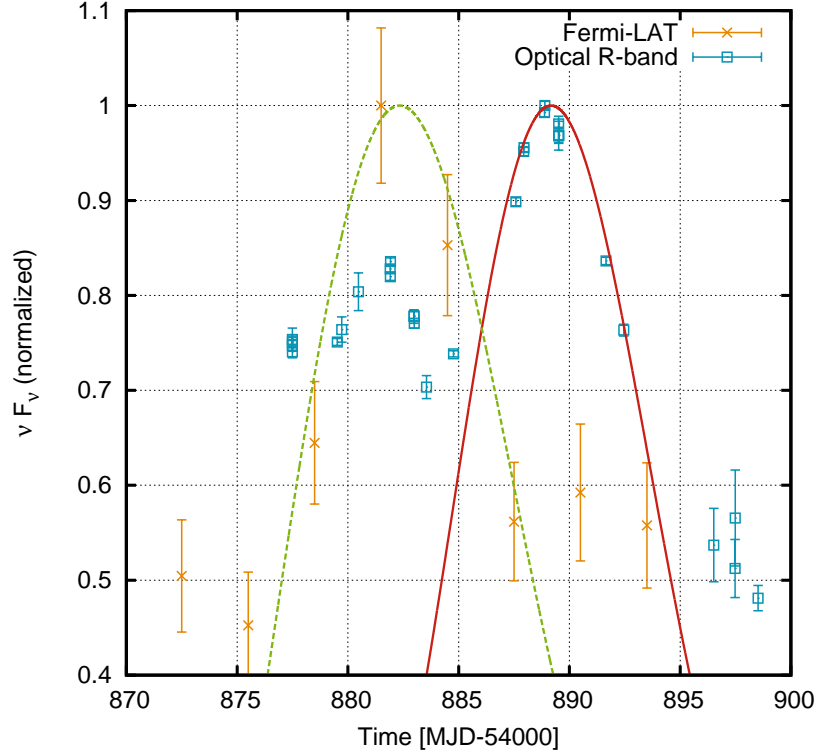


**Figure 7.** The February 2009  $\gamma$ -ray/optical outburst of blazar 3C 279 (from Abdo et al. 2010d; Hayashida et al. 2012) with a time lag of  $\approx 10$  days in normalized units. Lines show our analytical model (*dotted line* — ERC flare; *solid line* — synchrotron flare) for parameter values  $q_m = 30$ ,  $\beta_B = 2$ ,  $\beta_E = 5$ ,  $\sigma = 1$ ,  $r_m = 4.4$  pc and  $\Gamma = 10$ .